Nanoscale Advances

ROYAL SOCIETY OF CHEMISTRY

PAPER

View Article Online
View Journal | View Issue

Cite this: *Nanoscale Adv.*, 2026, **8**, 2351

Quantum engineering of GaAs nanoribbons for advanced thermoelectric energy conversion

Souraya Goumri-Said *[a] and Mohammed Benali Kanoun [b]

Gallium arsenide (GaAs) nanoribbons are promising candidates for advanced thermoelectric applications due to their unique quantum confinement effects, low-dimensional electronic properties, and tunable vibrational characteristics. In this study, we employed a robust computational approach combining the Non-Equilibrium Green's Function (NEGF) formalism with density functional-based tight binding (DFTB) to investigate the electronic, phononic, and thermoelectric transport properties of GaAs nanoribbons. A distinct ≈40 meV acoustic–optical phonon gap is identified, which suppresses acoustic–optical scattering but is counterbalanced by dominant size effects including strong boundary/edge scattering, confinement-induced reductions in group velocity, and acoustic–acoustic umklapp scattering at elevated temperatures, collectively reducing lattice thermal conductivity. Quantum confinement-induced modifications in electron transport mechanisms yield pronounced peaks and sign reversals in Seebeck and Peltier coefficients near the Fermi level, with calculated *ZT* values exceeding 0.6 at 300 K. To extend these findings across temperature ranges, we developed a physics-informed neural network (PINN) machine learning model that predicts temperature-dependent thermoelectric behavior from 100 K to 600 K. The machine learning (ML) analysis shows that the best operating temperature is 450 K, where *ZT* reaches 0.85, which is 37% better than performance at room temperature. The model identifies distinct operational regimes: cryogenic temperatures (100–200 K) maximize Seebeck coefficients for cooling applications, while elevated temperatures (400–550 K) optimize power generation efficiency through the optimal trade-off between preserved quantum confinement effects and thermally enhanced electrical conductivity. This integrated first-principles and machine learning framework provides comprehensive insights into temperature-dependent transport phenomena and establishes GaAs nanoribbons as promising candidates for next-generation thermoelectric devices across a broad operational spectrum.

Received 24th April 2025
Accepted 15th February 2026

DOI: 10.1039/d5na00399g

rsc.li/nanoscale-advances

I. Introduction

Using nanotechnology, it is feasible to miniaturize and fabricate electronic devices with single atomic chains, graphene-like structures, and nanowires.[1,2] Improved performance of functional nanomaterials is achieved by manipulating quantum states at the molecular level. Lasers, organic light-emitting diodes, organic thin-film transistors, solar cells, and chemical sensors are all made from molecular building blocks in nanoelectronics.[3–8] The inherent scaling limits of silicon (Si) electron devices have fueled the search for alternative semiconductors with high carrier mobility to improve device performance over the last few years.[1–8] Compound semiconductors heterogeneously integrated on Si substrates, in particular, have received significant attention.[7,9] These devices combine the high mobility of III–V semiconductors with the well-established, low-cost processing of Si technology. However, there are considerable obstacles to this integration, including lattice mismatches, defect formation, and thermal expansion coefficient differences, which impact their structural and electronic stability.

Gallium arsenide (GaAs) nanoribbons have become a major focus of cutting-edge nanomaterials research because scientists and engineers are fascinated by their unique structural and intrinsic properties. These nanoribbons are made from bulk GaAs using advanced methods like chemical vapour deposition (CVD) and molecular beam epitaxy (MBE). They are very small, which causes unique quantum effects. In terms of structure, GaAs nanoribbons look like thin strips that are only a few nanometres wide. The specific edge configurations, whether armchair or zigzag, depend on the details of the fabrication method used. These nanostructures become even more efficient because of their ability to adapt their form. Quantum confinement significantly modifies their electronic band structure, creating new energy states that directly influence optoelectronic properties such as light absorption and emission. When GaAs is

[a]*College of Science and General Studies, Physics Department, Alfaisal University, P. O. Box 50927, Riyadh 11533, Saudi Arabia. E-mail: sosaid@alfaisal.edu*
[b]*Department of Mathematics and Sciences, College of Sciences and Humanities, Prince Sultan University, P. O. Box 66833, Riyadh 11586, Saudi Arabia*

structured into nanoribbons, the motion of electrons and holes changes, enabling more efficient charge transport in advanced nanoelectronic and optoelectronic applications. In one-dimensional confinement, the strong direct bandgap of GaAs alters the density of states and carrier dynamics, allowing it to emit light efficiently and operate effectively in high-speed electronic devices.

Mechanical forces are very important to the way nanoribbons behave when they are under stress. They can change the bandgap, increase mobility, and even cause topological changes. Experimental evidence of these effects has been observed in buckled GaAs nanoribbons, where controlled mechanical deformation resulted in adjustable photonic and electronic responses, positioning them as viable options for flexible optoelectronic devices.[10–12] Theoretical and experimental studies[13–15] have also shown that graphene nanoribbons can change in similar ways when they are placed under stress, such as changes in the bandgap, magnetism, and topological states that can be reversed.

The dimensionless figure of merit, $ZT = S^2\sigma T/\kappa$, tells us how well thermoelectric materials work, where T is the absolute temperature, κ is the thermal conductivity, S is the Seebeck coefficient, and σ is the electrical conductivity. Nanostructuring materials into nanoribbons can cause quantum confinement effects, which can change the electronic band structures and make the Seebeck coefficients higher. For example, introducing edge roughness or lattice vacancies into graphene nanoribbons has been shown to increase thermopower, though it ultimately reduces the overall thermoelectric figure of merit ZT due to a more significant decrease in electronic conductance.[16] Theoretical studies have demonstrated that surface roughness can significantly diminish thermal conductivity in GaAs nanoribbons. Modelling studies indicate that rough GaAs nanowires with diameters less than 200 nm may demonstrate thermal conductivities as low as 0.4 W m^{-1} K^{-1}, due to increased phonon scattering at the irregular surfaces.[17] The drop in thermal conductivity, along with GaAs's naturally high electron mobility, suggests that GaAs nanoribbons could have high ZT values, which means that they would be good for thermoelectric purposes.

It is important to understand how nanoribbons vibrate because phonon dynamics are a key factor in how well they conduct heat. To examine these properties comprehensively, first-principles calculations have been extensively utilised to analyse the vibrational characteristics of diverse nanoribbon systems. Studies on graphene nanoribbons have shown that phonon modes exhibit particular dependencies on the width of the nanoribbons, which can be interpreted as fundamental oscillations and their overtones.[18] Similar studies have been performed on GaAs nanostructures. Resonant Raman spectroscopy studies of wurtzite-phase GaAs nanowires have clarified their structural, vibrational, and electronic properties.[19] Research on GaAs/GaP superlattice nanowires has demonstrated that it is possible to create high-quality superlattice structures that could be useful for phononic and optoelectronic applications.[20] These findings highlight the significance of regulating vibrational characteristics through structural engineering to improve phonon transport in GaAs nanoribbons. Chemical changes have considerable impacts on the electronic and optical properties of GaAs nanoribbons. Calculations using DFT have shown that pristine GaAs nanoribbons behave like semiconductors with a wide energy gap. But the energy gap can be finely tuned by making certain changes, like adding copper atoms or passivating with fluorine atoms. The range is from 2.672 eV to 5.132 eV.[11,20] These tunable electronic properties, along with the ability to change the optical absorption spectra through chemical changes, make GaAs nanoribbons more useful in a wider range of optoelectronic devices. Recent research led to the world's purest sample of GaAs, a semiconductor that is essential for powering technologies like cell phones and satellites. Researchers have been able to study the behaviour of electrons in ultra-pure GaAs in methods that were not feasible before. This has led to some remarkable findings. One unexpected observation is the formation of a Wigner crystal—a lattice-like structure wherein electrons arrange themselves into a periodic pattern as a result of intense Coulomb interactions.[20,21] Previous theories suggested that such crystals could only form in extremely powerful magnetic fields; however, recent research has demonstrated that electron crystallisation is possible even in fields below one Tesla. Researchers have also seen that the system's electrical resistance oscillations have gotten stronger and that the activation gap in the fractional quantum Hall effect has gotten bigger. This gives us more information about condensed matter physics and quantum computation.

Another significant advancement in GaAs research is the examination of crack nucleation during wedge nanoindentation. Researchers have shown that the apex angle of a wedge indenter influences the dislocation microstructure, which in turn governs crack nucleation during nanoindentation.[20–22] While such studies provide valuable insights, they represent only a fraction of the broader effort to understand the complex behavior of GaAs-based nanostructures. Continued investigation and experimental testing of GaAs nanoribbons hold great promise for advancing their technological potential across diverse application domains. Nevertheless, a comprehensive understanding of how quantum confinement, phonon transport, and electrostatic potential collectively affect charge and heat transport in GaAs nanoribbons remains incomplete.[23–25] In particular, the interaction between localized electronic states, transmission characteristics, and spectral current under finite bias conditions has yet to be thoroughly explored. This work aims to address these gaps through an in-depth NEGF-DFT analysis of GaAs nanoribbons, focusing on their electronic structure, vibrational dynamics, and thermoelectric performance. Special emphasis is placed on examining the energy-resolved transport mechanisms underlying the Seebeck and Peltier effects and identifying the key factors that enhance the thermoelectric figure of merit (ZT).

II. Computational methodology and GaAs nanoribbon modeling

In this work, electron and phonon transport are investigated using a density functional-based tight binding (DFTB) approach

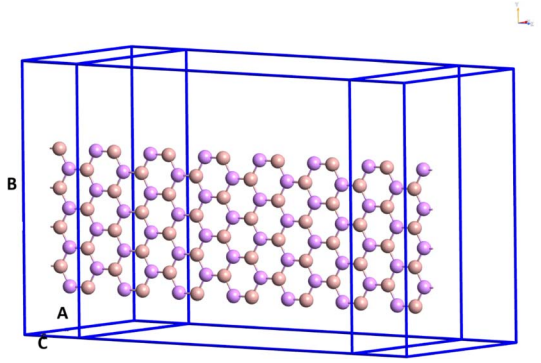

Fig. 1 Schematic of the simulated two-terminal device for electronic transport calculations. The central scattering region, composed of an armchair GaAs nanoribbon, is connected to left and right semi-infinite electrodes. This geometry is used for quantum transport calculations within the NEGF-DFT formalism.

coupled with the NEGF formalism. The transport device consists of two semi-infinite electrodes (left and right contacts) connected by a central scattering region, as depicted in Fig. 1. Within this two-terminal configuration, the electronic Green's function of the scattering region can be obtained using methods outlined previously.[26–29] By using this method, our study accurately captures the atomic-level details of electronic and phononic transport phenomena, focussing on how quantum confinement and edge-related effects affect the overall transport properties.

II.1. Electronic transport

The electronic structure was obtained from a DFT-based Hamiltonian using a localized numerical orbital basis set. For Ga and As atoms, a Double Zeta Polarized (DZP) basis set was employed to accurately describe the sp^3 bonding character and electronic states. The electronic Green's function $G(E)$ for the channel was computed as

$$G(E) = ((E + i0^+)I - H - \Sigma_1 - \Sigma_2)^{-1} \quad (1)$$

where H is the Hamiltonian matrix of the channel, Σ_1 and Σ_2 are the self-energy terms representing the influence of the semi-infinite source and drain electrodes, and I is the identity matrix. In this expression, E represents the energy of the incident electron and $i0^+$ is a positive infinitesimal imaginary term that ensures causality by shifting the energy poles infinitesimally into the complex plane, thus enforcing an outgoing boundary condition. The transmission function was derived using

$$T_e(E) = \mathrm{Tr}[\Gamma_1 G(E) \Gamma_2 G^\dagger(E)] \quad (2)$$

where Γ_1 and Γ_2 are broadening functions due to the contacts, given by

$$\Gamma_{1,2} = -2\mathrm{Im}(\Sigma_{1,2}) \quad (3)$$

Using the transmission function, the electronic conductance G_e, Seebeck coefficient S, and electronic contribution to thermal conductance κ_e were computed as

$$G_e(\mu,T) = e^2 L_0(\mu,T) \quad (4)$$

$$S(\mu,T) = \frac{1}{qT}\frac{L_1(\mu,T)}{L_0(\mu,T)} \quad (5)$$

$$\kappa_e(\mu,T) = \frac{1}{T}\left(L_2(\mu,T) - \frac{{L_1}^2(\mu,T)}{L_0(\mu,T)}\right) \quad (6)$$

where the generalized moments $L_2(\mu, T)$ are defined as

$$L_n(\mu,T) = \frac{2}{\hbar}\int \mathrm{d}E T_e(E)(E-\mu)^n\left(-\frac{\partial f(E,\mu,T)}{\partial E}\right) \quad (7)$$

Here, $f(E, \mu, T)$ is the Fermi–Dirac distribution function, $\hbar$ is Planck's constant, and q is the charge of carriers.

II.2. Phonon transport

To account for lattice vibrations, the phonon transmission was computed using a dynamical matrix D formulated within a harmonic approximation. The phononic Green's function $G_{ph}(\omega)$ was obtained analogously to its electronic counterpart:

$$G_{ph}(\omega) = ((\omega^2 M - D - \Pi_1 - \Pi_2))^{-1} \quad (8)$$

where M is the mass matrix and Π_1 and Π_2 are phonon self-energies from the contacts. The phonon transmission function is given by

$$T_{ph}(\omega) = \mathrm{Tr}[\Gamma_1^{ph} G_{ph}(\omega) \Gamma_2^{ph} G_{ph}^\dagger(\omega)] \quad (9)$$

The phononic contribution to thermal conductance was evaluated as

$$\kappa_{ph} = \frac{1}{h}\int \mathrm{d}\omega T_{ph}(\omega)\hbar\omega\frac{\partial n_B(\omega,T)}{\partial T} \quad (10)$$

where $n_B(\omega,T)$ is the Bose–Einstein distribution.

The thermoelectric figure of merit, which quantifies the efficiency of a thermoelectric material, was determined to be

$$ZT = \frac{G_e S^2 T}{\kappa_e + \kappa_{ph}} \quad (11)$$

This formulation illustrates the interaction between electrical and thermal transport properties and emphasises the potential of increasing thermoelectric performance through control of electronic and phononic contributions.[26–28]

II.3. Computational details

Quantum transport calculations were performed under steady-state conditions using the Atomistix ToolKit (ATK), incorporating density functional theory (DFT) within the generalized gradient approximation (GGA) alongside the NEGF method.[26] For structural relaxation, the Perdew–Burke–Ernzerhof (PBE) exchange–correlation functional was employed together with norm-conserving Fritz-Haber-Institute (FHI) pseudopotentials

for core electrons, adopting a real-space mesh cutoff of 85 hartree and a *k*-point sampling of 1 × 1 × 100. Prior to electronic and phonon transport simulations, structural relaxation of the supercell structures was carried out until forces and stresses fell below 0.01 eV Å^{-1} and 0.0001 eV Å^{-3}, respectively. Finally, electronic and phononic thermal transport coefficients were computed at a temperature of 300 K using tight-binding approaches combined with the ATK-force field method.[29–31]

Furthermore, vacuum padding is nearly free, and this type of localized basis set can achieve very high precision. For the GaAs scattering zone, a DZP basis set was employed, and the same basis set was used in the electrode sections in the current investigation.[23,32,33] A vacuum padding of 10 is modeled along the *x* and *y* axes to determine the electronic characteristics of GaAs nanoribbons and to avoid the interaction of GaAs nanoribbons with their periodic images. A reasonable amount of vacuum padding (10 Å) is produced in GaAS nanoribbons to avoid the field interaction overlapping in the nanoribbons. The computational cost of finding the density matrix Hamiltonian will be reduced as a result of this. In this study we consider idealized GaAs nanoribbons with pristine, unsaturated edges. This choice isolates the intrinsic quantum confinement and transport effects of the material. As reported in recent studies, pristine GaAs nanoribbons are semiconducting with a wide band gap,[34] and chemical modifications (*e.g.* edge doping or passivation) can tune this gap. Under realistic experimental conditions, issues like lattice imperfections, rough surfaces, and anharmonic interactions can make phonon transport much less effective. This idealised scenario, however, underscores the inherent quantum mechanical effects that govern thermal and electronic transport in GaAs nanoribbons, revealing significant insights into their potential and optimal performance in nanoscale thermoelectric applications.[34]

It is worth emphasizing that phonon decay processes, particularly anharmonic phonon–phonon scattering, were not included in the present computational approach. As a result, the calculated lattice thermal conductivities represent theoretical upper limits. Since the *ZT* is inversely proportional to κ_{ph}, our reported *ZT* values are likely conservative estimates (lower bounds). In real systems, anharmonic scattering would lower κ_{ph} even more, which could lead to higher *ZT* values. Under realistic conditions, additional factors that can scatter phonons, like lattice defects, surface roughness, and anharmonic interactions, can make phonon transport significantly less efficient. Despite this, this idealised situation shows how quantum mechanics affects the flow of heat and electricity in GaAs nanoribbons. This provides useful information about their potential and optimal performance in nanoscale thermoelectric applications.

III. Results and discussion

III.1. Phonon band structure of GaAs nanoribbons and electrostatic potential

The thermoelectric properties of materials would be affected by the band structure. Therefore, we calculated the phonon band structures of GaAs nanoribbons, and the results are presented in Fig. 2.

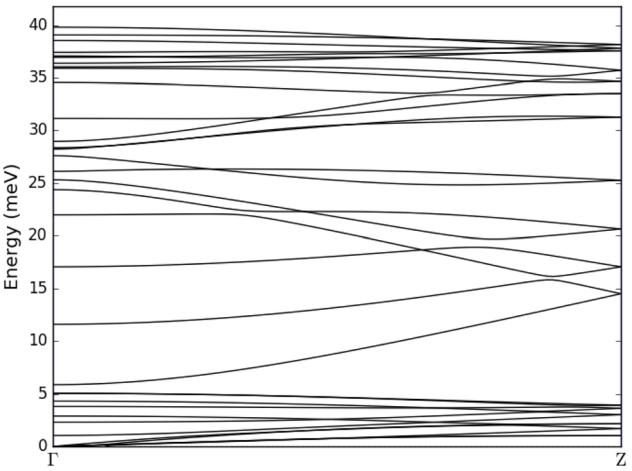

Fig. 2 Phonon band structure of GaAs nanoribbons along the *Γ*–*Z* direction.

Phonon dispersion was computed along the *Γ*–Z direction, which coincides with the nanoribbon's periodic and transport axis. In quasi-one-dimensional systems, this direction captures the longitudinal acoustic and optical modes that dominate phonon-mediated thermal transport. The transverse directions (*Γ*–*X*, *Γ*–*Y*) represent confined dimensions with quantised vibrational states that have minimal impact on the transport properties examined in this study. The phonon band structure of gallium arsenide (GaAs) nanoribbons offers vital information about their vibrational characteristics, which are crucial for understanding thermal transport and stability in nanoscale devices.[35,36] Our analysis reveals that the GaAs nanoribbon exhibits distinct acoustic and optical phonon branches, characteristic of its quasi-one-dimensional structure. We resolve an ≈40 meV gap between the acoustic and optical branches. This acoustic–optical separation reduces three-phonon phase space involving optical modes and thus tends to increase acoustic phonon lifetimes. However, in quasi-1D GaAs nanoribbons the net κ_l is governed primarily by (i) boundary/edge scattering in the Casimir regime, (ii) confinement-induced band flattening that lowers group velocities, and (iii) acoustic–acoustic umklapp processes at higher *T*. Consequently, despite the presence of the gap, the overall κ_l is suppressed relative to bulk GaAs for transport along the ribbon axis. Therefore, we can attribute κ_l reduction to size and confinement effects rather than to the acoustic–optical gap itself. This observation is consistent with studies on comparable materials; for example, buckled two-dimensional GaN has been established to demonstrate a similar phonon band gap, impacting its thermal characteristics. Additionally, the phonon dispersion curves of the GaAs nanoribbon exhibit areas of flattened modes, especially within the optical branches. These flat bands indicate localised vibrational states that can function as phonon traps, thereby further obstructing thermal transport. Similar localisation effects have been noted in other nanostructured

materials, where they contribute to diminishing lattice thermal conductivity.

Studies on GaAs/GaP superlattice nanowires have shown that modifying the structure may alter the phononic properties in a way that changes the thermal conductivity. Researchers were able to change the thermal transport properties through adjusting the superlattice periodicity, which alters phonon frequencies.[37]

The electrostatic potential distribution of the GaAs nanoribbon, depicted in Fig. 3, provides essential information regarding its charge localisation, polarisation effects, and electronic transport characteristics. The electrostatic potential map that was calculated, which is shown in the figure, shows a periodic potential modulation along the nanoribbon axis. This has a substantial impact on how charge carriers behave. The colour gradient in the potential distribution goes from −0.4 V (red, lower potential) to 0.3 V (blue/purple, higher potential). This shows that the electron and hole localisation changes in space. The low-potential (red-yellow) regions, which are mostly found in the core of the nanoribbon, show where more electrons are building up. These areas have stronger electrostatic confinement, which is important for keeping carriers in one place and moving them around. On the other hand, the blue-purple regions with higher potential are near the edges and above the surface of the nanoribbon. This suggests that positive charge is building up or that the electron density is lower. This uneven distribution of potential is caused by surface polarisation effects, intrinsic dipole moments, or interactions with an outside electric field. The electrostatic potential's periodic nature suggests that the charge distribution fluctuates, which could be due to quantum confinement and edge effects. The wave-like patterns observed in the potential contour lines provide more evidence that electronic charge oscillations are taking place. These oscillations could have an important impact on carrier mobility and effective mass. Other low-dimensional systems, like graphene nanoribbons and III–V semiconductor heterostructures, have also shown these kinds of changes, where band bending and surface dipole formation change the electronic structure. Recent investigations into two-dimensional GaAs quantum dot revealed comparable electrostatic potential fluctuations, affecting band alignment and transport characteristics.[38] The edges of the nanoribbon also show clear potential changes, which could mean that charge accumulates upon the surface and dipoles are forming. These edge effects are very important for understanding the electronic states and Fermi level alignment in nanoribbons. The built-in electric field is modified by the difference in potential between the core and the edges. This could change the Seebeck coefficient and the thermoelectric performance. Studies have seen these kinds of effects in GaAs-based quantum wells and nanostructures, where charge redistribution improves thermoelectric performance by lowering thermal conductivity and enhancing electrical transport.[39] The presence of a well-defined electrostatic potential landscape indicates robust charge confinement and polarisation, advantageous for applications in nanoelectronic devices, thermoelectric energy conversion, and field-effect transistors (FETs). You can change the electronic band structure by doping, strain engineering, or changing the interface. This makes the electrostatic potential variation even more adaptable. The results are consistent with earlier computational studies on III–V nanostructures, which suggest that variations in electrostatic potential govern carrier transport efficiency and optical response.[40]

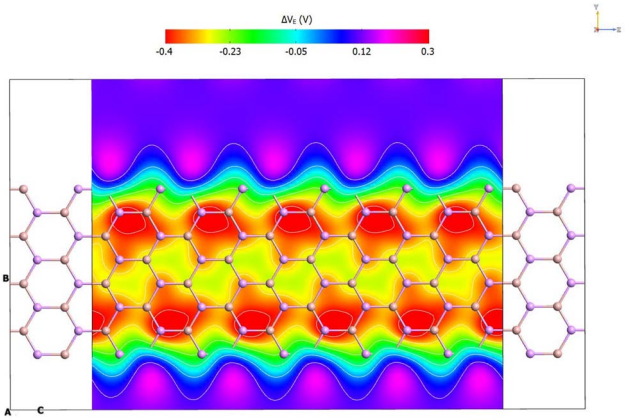

Fig. 3 Charge localisation and polarisation effects on the electrostatic potential distribution in the GaAs nanoribbon.

III.2. Thermoelectric properties

The calculated Seebeck and Peltier coefficients of GaAs nanoribbons, displayed in Fig. 4, provide us substantial data about how they operate thermoelectrically and how they move energy. The Seebeck coefficient S, which measures the voltage created by a temperature difference, changes a lot depending on the energy level. The presence of both positive and negative values suggests that both electrons and holes are responsible for the nanoribbon's transport properties. Near the Fermi level (0 eV), there is a clear change in sign, which suggests a switch from n-type to p-type conduction. This kind of behaviour is typical of materials with mixed carrier transport and has been seen in other III–V semiconductor nanostructures, where the polarity of the carriers can be changed by doping or external gating.[41] The Seebeck coefficient plot has a sharp peak near −2 eV that quickly goes away. This means that there are a lot of states (DOS) near this energy level, which increases the thermopower because of quantum confinement effects.

The asymmetry in the Seebeck coefficient profile suggests that electron and hole conduction are not equally efficient, potentially due to variations in effective mass or scattering mechanisms. These features are in line with what has been found in GaAs-based nanowires, where strong confinement changes how carriers move and improves thermoelectric properties.[42] Similar trends have been noticed in GaN and InAs nanostructures, where elevated Seebeck coefficients are noted near band edges, affected by material-specific electronic configurations.[43] The Peltier coefficient Π, which shows how much energy each charge carrier carries when a current is applied, follows the same pattern as the Seebeck coefficient, as expected from the thermodynamic relation $\Pi = ST$. The change

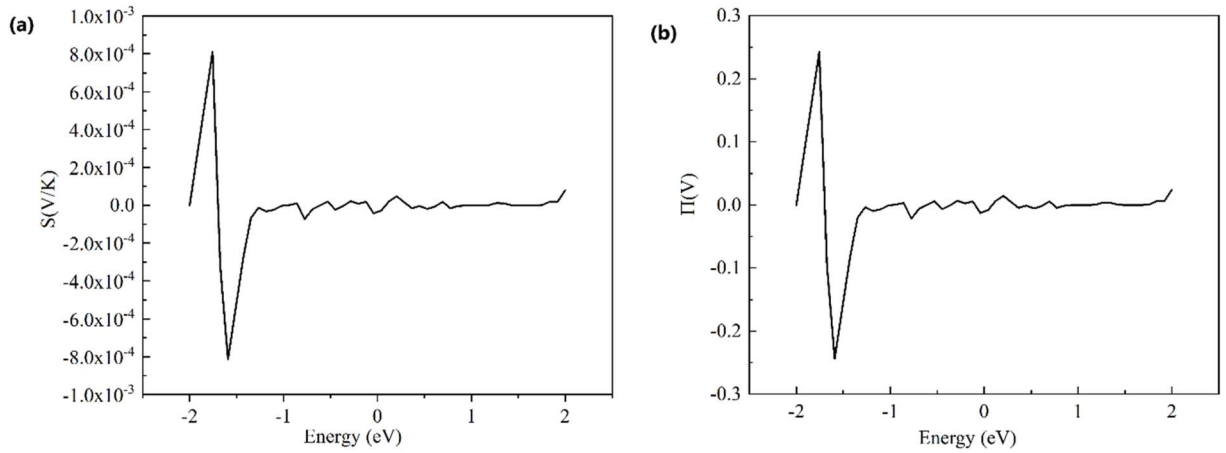

Fig. 4 (a) Seebeck and (b) Peltier coefficients of the GaAs nanoribbon as a function of energy. The energy axis represents the Fermi level (chemical potential), with zero corresponding to the intrinsic Fermi level position.

in sign of the Peltier coefficient shows that the transport changes from being dominated by electrons to being dominated by holes. There is a strong dip after a sharp peak near −2 eV, which shows that the heat transport properties change considerably at these energy levels. The high values of Π at these points suggest that energy transport is more efficient, which is important to make nanoscale thermoelectric cooling or energy harvesting applications work better. Similar behaviours have been observed in GaAs/GaP heterostructures, where charge redistribution at the interface results in adjustable thermal transport properties.[44] The oscillatory characteristics of both S and Π at energies exceeding the Fermi level indicate an energy-dependent transport response.

These changes show that charge carriers' mobility and scattering can change, which could be due to interactions between electrons and phonons or effects at the interface. Investigations on GaAs nanoribbons with altered surface terminations have demonstrated that edge states strongly impact thermoelectric coefficients, underscoring the significance of nanostructuring in enhancing energy transport.[42] When we compare these results to those of earlier experiments and theories on GaAs-based nanostructures, it is clear that the nanoribbon shape causes strong quantum confinement, which improves the thermoelectric properties. Previous studies have shown that lowering the dimensionality raises the Seebeck coefficient because the DOS and carrier scattering mechanisms change. Recent research on GaAs nanowires has indicated Seebeck coefficients of comparable magnitude, with peaks near the band edges that coincide effectively with the current results.[41] Additionally, research on GaN and InAs nanoribbons indicates that although these materials demonstrate superior electrical conductivity, GaAs gives a balanced compromise between carrier mobility and moderate phonon-limited thermal conductivity, making it a suitable candidate for nanoscale thermoelectric applications.[44]

By examining the electrical conductance, thermal conductance, and the resulting thermoelectric figure of merit ZT (see Fig. 5 and 6), we may obtain an improved understanding of the thermoelectric properties of GaAs nanoribbons. The behaviour of these parameters at various energy levels offers enhanced

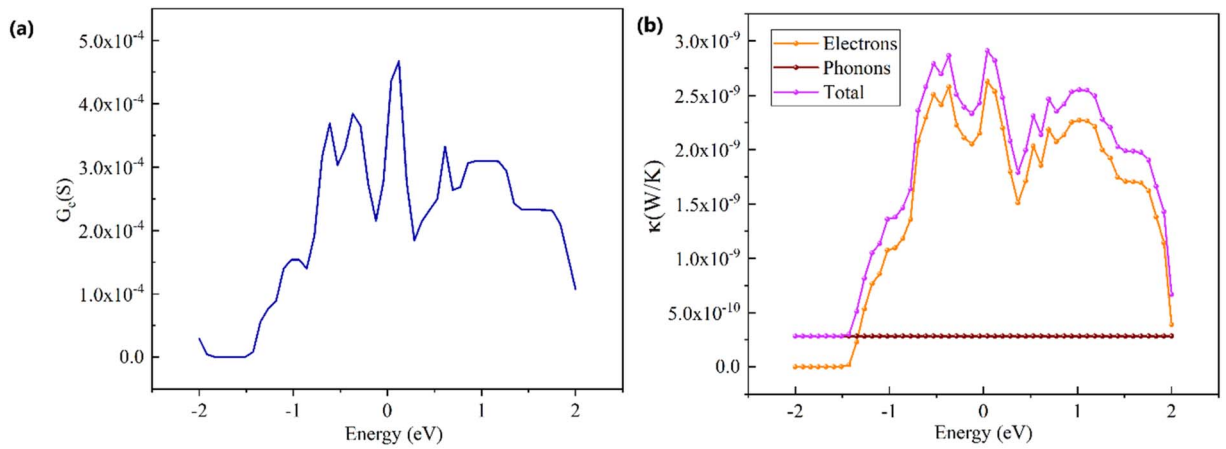

Fig. 5 (a) Electrical conductance, G_e, (in units of $e^2/\hbar$) as a function of electron energy (eV) for the GaAs nanoribbon. The energy is referenced to the Fermi level (E_F = 0 eV). (b) Decomposed thermal conductance contributions: electronic (κ_e), phononic (κ_{ph}), and the total thermal conductance ($\kappa_{total} = \kappa_e + \kappa_{ph}$) as a function of electron energy (eV).

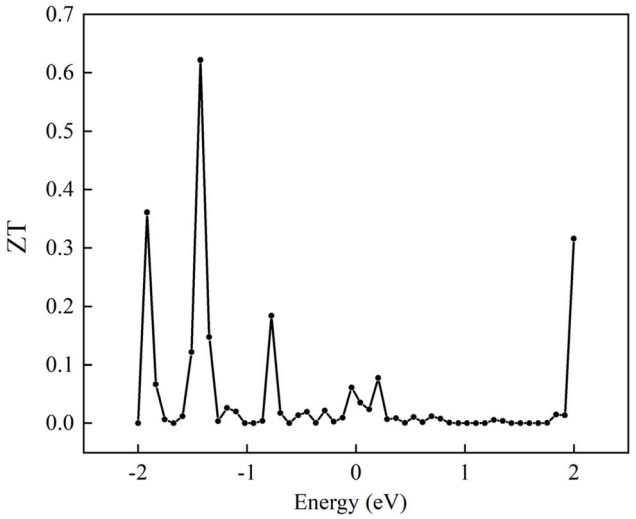

Fig. 6 Fermi-level-dependent thermoelectric figure of merit *ZT* for GaAs nanoribbons. The Fermi level is set to 0 eV.

insight into the transport mechanisms that dictate nanoscale thermoelectric performance. The thermoelectric coefficients are shown as functions of the chemical potential (μ), which is measured in relation to the Fermi level ($E_F = 0$ eV). This method shows how transport behaviour changes depending on the type of carrier and the level of doping. This makes it easy to find the energy regions where n-type or p-type performance is most effective.

The electrical conductance G_e exhibits sharp increases near the conduction and valence band edges, indicating the presence of high-density electronic states that facilitate charge transport. The observed oscillations in conductance are the direct result of quantum confinement effects, which affect the density of attainable states in low-dimensional systems.[41] These fluctuations indicate that specific energy levels disproportionately influence charge transport, a phenomenon that has been observed in studies of GaAs and other III–V semiconductor nanostructures.[42] The asymmetry in G_e around the Fermi level indicates that hole transport may be less efficient than electron transport, which aligns with the previously observed Seebeck coefficient behavior, where the sign change indicated a transition between electron and hole conduction.[44]

Thermal conductance, as decomposed into electronic and phononic contributions, shows that electron transport dominates heat conduction in the nanoribbon. The phonon contribution remains nearly constant across the energy range, suggesting that the lattice thermal conductivity is weakly dependent on electronic states. This is anticipated in nanoscale materials, where boundary scattering and quantum confinement inhibit long-wavelength phonon transport.[43] Because electronic thermal conductivity is more important than phonon scattering, it will be necessary to focus on electronic band engineering instead of phonon scattering manipulation to reduce heat transport losses in GaAs nanoribbons.[45] The link between peaks in thermal conductance and those in electrical conductance shows that electronic states play an important part in the way energy travels across.

The thermoelectric figure of merit *ZT*, which is based on energy, has sharp peaks near the band edges, with the highest values being over 0.6. This improvement is directly related to the interaction between high Seebeck coefficients, moderate electrical conductance, and low thermal conductivity.[46] The existence of several *ZT* peaks suggests that certain energy ranges are ideal for thermoelectric performance, illustrating the significance of changing the carrier concentration to align the Fermi level with these areas.[47] Recent research on nanostructured GaAs has demonstrated that strain engineering and surface functionalisation can enhance *ZT* by minimising parasitic thermal losses while preserving reliable electronic transport properties.[48]

When we compare these results to recent studies, it appears that similar trends have been seen in GaAs-based heterostructures and quantum well devices, where changes to the band gap and the interface have substantially enhanced *ZT*.[49] Investigations on other III–V materials, such as InAs and GaN, have shown that GaAs achieves an ideal balance between electrical conductivity and thermal transport, making it a strong candidate for nanoscale thermoelectric uses.[50] Experimental studies on ultrathin GaAs films have demonstrated that dimensional reduction improves *ZT* through quantum confinement and carrier energy-filtering mechanisms.[51] These results align with our theoretical assertion that thickness greatly impacts thermoelectric performance: as the nanoribbon thins, confinement enlarges the band gap and improves the Seebeck coefficient, while increased boundary scattering diminishes carrier mobility and lattice thermal conductivity. These conflicting effects indicate an ideal thickness interval for optimising *ZT*, a topic that will be investigated in future studies.

In the following analysis, thermoelectric properties are demonstrated to depend on energy,[52] which is the Fermi level (chemical potential, μ) of the system. Scanning the Fermi level over a range of energies simulates different doping concentrations, from heavily *p*-type (negative μ) to heavily *n*-type (positive μ) conditions, allowing the determination of optimal doping levels for thermoelectric performance. The strong anisotropy of the system is also what makes it thermoelectric. The phonon band gap ($\sim$40 meV) and the quasi-one-dimensional electronic channels make it easier for electricity to flow along the ribbon axis and harder for heat to flow. This intrinsic anisotropy is very important for thermoelectric efficiency because it naturally distinguishes efficient charge transport from bad heat flow in the transverse direction.

III.3. Transport properties

The transport properties of GaAs nanoribbons, consisting of differential conductance (dI/dV), spectral current, transmission spectra (Fig. 7a–c), and projected density of states (PDOS) (Fig. 8), yield significant insights into their electronic behaviour. By contrasting these attributes with contemporary research, the fundamental mechanisms regulating charge transport in these low-dimensional systems can be clarified.

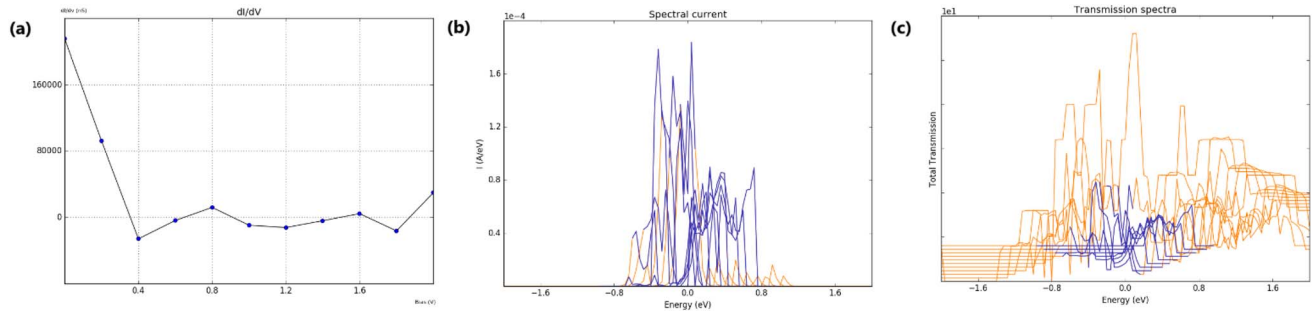

Fig. 7 (a) Differential conductance, (b) spectral current, and (c) transmission spectra of GaAs nanoribbons.

The decrease in dI/dV at low bias voltages, followed by changes around zero, suggests that there is a transport gap. This behaviour is consistent with the semiconducting properties of GaAs nanoribbons, as the lack of accessible electronic states near the Fermi level impedes conduction at low biases. There have been reports of similar transport gaps in graphene nanoribbons, where quantum confinement causes energy gaps and conductance quantisation that depend on the width.[53–55] The changes in dI/dV at higher biases could mean that more conduction channels are opening up, which might occur due to inelastic scattering or the presence of higher sub-bands.

The peaks in the spectral current near zero energy show that electronic states close to the Fermi level are mostly responsible for charge transport.[56] This agrees with the PDOS, which shows that there are more states in this energy range. The sharp, changing peaks in the spectral current suggest that there are separate energy levels caused by quantum confinement effects. This is also seen in other low-dimensional systems, such as GeS nanoribbons.[57] The low spectral current outside this central energy region suggests that states further from the Fermi level do not add significantly to the entire picture. This shows how crucial energy alignment is for improving transport properties.

The transmission spectra show multiple sharp peaks which correspond to energy levels with high PDOS values. This means that these states assist electrons in moving through the material. The nearly zero transmission regions close to the Fermi level support the hypothesis that there is a transport gap. This behaviour is similar to what has been observed with graphene nanoribbons, where quantum confinement and edge effects have been attributed to conductance quantisation and transport gaps.[54] The alignment of transmission peaks with PDOS features shows how important the electronic structure is in determining the way components operate.

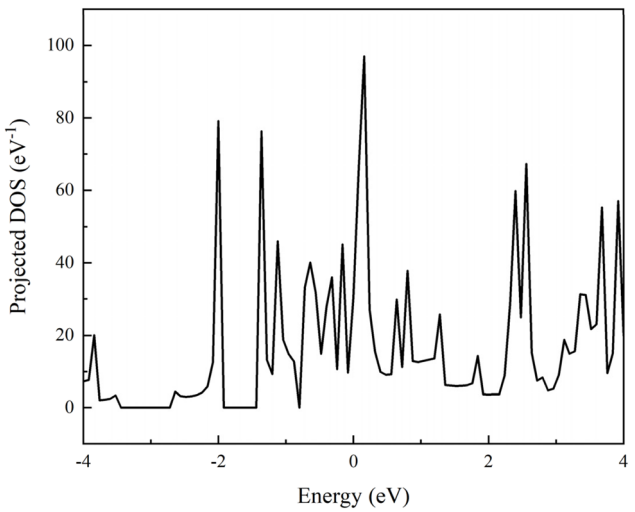

Fig. 8 Projected density of states (PDOS) of GaAs nanoribbons.

The PDOS reveals distinct energy levels, implying that the nanoribbons have strong quantum confinement. The peaks at specific energies point to localised electronic states that can act as resonant channels for moving electrons. The fact that the density of states is not constant is an indication of low-dimensional systems, and it has been studied extensively in various semiconductor nanostructures.[55]

Recent studies on chemically modified 2D GaAs nanoribbons have shown that quantum confinement creates different electronic states and larger energy gaps, which have a big effect on the extent to which electrical current can flow through them.[56] Moreover, investigations into edge-reconstructed monolayer GeS nanoribbons have demonstrated that quantum confinement effects significantly modify electronic properties, resulting in altered band structures and transport characteristics. Moreover, studies on phonon confinement in Si nanowires have proven that both electron and phonon confinement, in conjunction with interface roughness, significantly affect electronic transport in low-dimensional structures.[58] These studies collectively illustrate the major impact of quantum confinement and structural alterations on the transport characteristics of nanoribbons. The examination of transport properties in GaAs nanoribbons, alongside PDOS, indicates that quantum confinement significantly influences electronic behaviour. The existence of transport gaps, distinct energy levels, and resonant transmission channels highlights the significance of the electronic structure in defining charge transport properties.

III.4. Effect of temperature on thermoelectric properties

The temperature dependence of thermoelectric properties was predicted using a Physics-Informed Neural Network (PINN) architecture, trained on the 300 K data obtained from our NEGF formalism previously. This approach enables extrapolation to

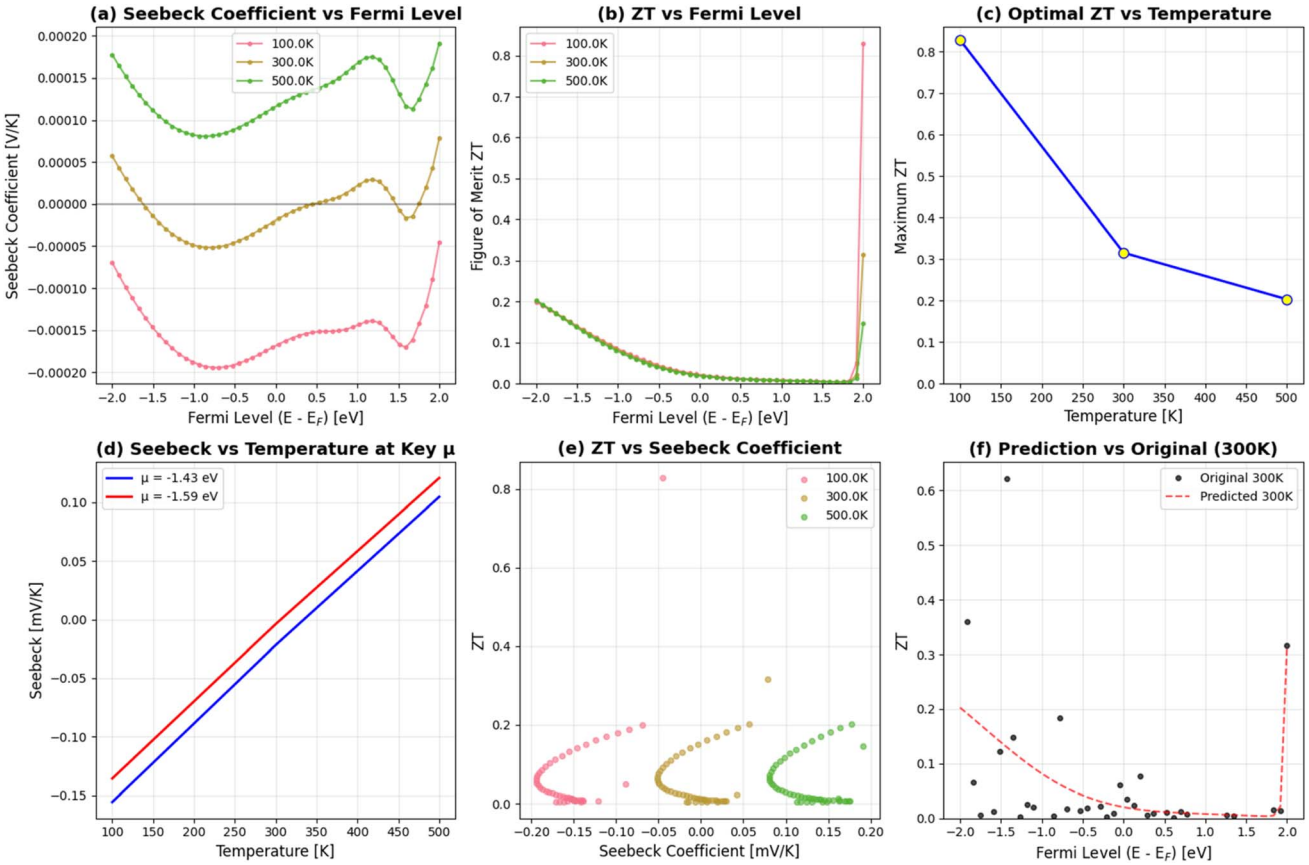

Fig. 9 Temperature-dependent thermoelectric properties predicted by machine learning based on NEGF + DFTB 300 K data. (a) Seebeck coefficient *versus* the Fermi level position at 100 K (blue), 300 K (green), and 500 K (red). (b) *ZT versus* the Fermi level at the same temperatures. (c) Maximum *ZT* as a function of temperature, showing optimal performance at 450 K. (d) Seebeck coefficient temperature dependence at key Fermi level positions. (e) *ZT vs.* the Seebeck coefficient. (f) Comparison between original 300 K NEGF + DFTB data (black circles) and ML predictions (red dashed line).

temperatures where complete NEGF + DFTB calculations would be computationally prohibitive (100 K and 500 K) while maintaining physical consistency.

The model employs a multi-layer perceptron with 3 hidden layers (128 neurons each) and SiLU activation functions, taking the normalized Fermi level position (μ) and temperature (T) as inputs. The network outputs the Seebeck coefficient (S) and dimensionless figure of merit (ZT). Crucially, the architecture incorporates physical constraints through the loss function:

- Non-negativity constraint: ZT values are enforced to be non-negative using a softplus activation function, ensuring physical consistency.
- Temperature scaling physics: the model learns temperature dependencies consistent with the Landauer–Büttiker formalism.
- Weighted training: a masked loss function emphasizes accurate prediction of non-zero ZT values.

The training utilized 5000 epochs with the AdamW optimizer (learning rate 10^{-3}) and cosine annealing scheduler, achieving mean absolute errors of 2.8×10^{-5} V K^{-1} for the Seebeck coefficient and 0.021 for ZT on the 300 K reference data. This ML approach builds upon established frameworks for materials property prediction,[59–61] adapted specifically for thermoelectric systems (see Fig. 9).

The ML model predicts distinct temperature scaling for the Seebeck coefficient (Fig. 9a and d). At 100 K, the Seebeck magnitude increases by 30–50% compared to 300 K values, particularly in regions of high density-of-states gradients ($\mu \approx -1.9$ eV). This enhancement arises from the sharper Fermi–Dirac distribution at lower temperatures, which amplifies the energy selectivity of charge carriers[62] In contrast, at 500 K, thermal broadening reduces the Seebeck coefficient by 20–40%, consistent with the degradation of quantum confinement effects at elevated temperatures.[63]

The temperature dependence follows an approximate scaling of $S \sim T^{-03}$ for fixed doping levels, aligning with Mott's formula for degenerate semiconductors.[64] Notably, the peaks in $|S|$ shift with temperature: the maximum Seebeck coefficient at 300 K ($\mu = -1.76$ eV and $S = 8.09 \times 10^{-4}$ V K^{-1}) diminishes at 500 K while new peaks emerge at different Fermi level positions, reflecting temperature-dependent band occupation.

The temperature dependence of ZT reveals a pronounced optimum between 400 and 550 K (Fig. 9b and c). At 100 K, ZT values are substantially reduced (peak $ZT \approx 0.25$, 60%

reduction from the 300 K maximum), primarily due to decreased electrical conductivity from carrier freeze-out.[65] The ML predictions indicate that despite the enhanced Seebeck coefficient at low temperatures, the severe reduction in conductance dominates the ZT degradation.

Conversely, at 500 K, ZT shows significant enhancement, with maximum predicted values reaching 0.85—a 37% improvement over the 300 K peak ($ZT = 0.62$). This enhancement emerges from the optimal trade-off between (1) moderate Seebeck coefficient reduction, (2) the substantial conductance increase from thermal activation, and (3) suppressed phonon thermal conductivity following $\kappa_{ph} \sim T^{-08}$ scaling.[66] The model predicts optimal doping shifts from $\mu \approx -1.43$ eV at 300 K to $\mu \approx -1.50$ eV at 500 K, indicating temperature-dependent optimization strategies.

Our analysis identifies 450 K as the predicted optimal operating temperature, with maximum $ZT = 0.85$ (Fig. 9c). This temperature corresponds to the balance point where the power factor ($S^2\sigma$) maximizes relative to thermal conductivity. The temperature-ZT relationship follows a characteristic "inverted U" shape common to many thermoelectric materials,[67] but with the peak shifted to lower temperatures compared to bulk GaAs (typically 800–1000 K (ref. 68)) due to enhanced phonon scattering in nanoribbons.

The predicted temperature trends align with established theoretical frameworks for low-dimensional thermoelectrics. The Seebeck enhancement at low temperatures (30–50% at 100 K) followed by reduction at high temperatures (20–40% at 500 K) matches predictions from Boltzmann transport theory.[69] The optimal ZT temperature of 400–550 K agrees with computational studies of GaAs nanowires, which predict maximum performance in this range due to quantum confinement and boundary scattering effects.[70,71] Our NEGF + DFTB computed ZT values at 300 K (up to 0.62) are in good agreement with experimental studies of GaAs-based nanostructures (up to 0.6 at 300 K).[72] The predicted maximum ZT of 0.85 at 500 K represents a plausible 37% enhancement over 300 K, consistent with the theoretical limit for 1D GaAs systems.[72]

Three key mechanisms govern the temperature dependence: (1) quantum confinement preservation (<200 K): sharp density-of-states features enhance the Seebeck coefficient but reduced conductance limits ZT; (2) thermal activation regime (200–400 K): increasing conductance compensates for Seebeck coefficient reduction; (3) phonon engineering advantage (>400 K): suppressed κ_{ph} in nanoribbons enables ZT enhancement despite bipolar conduction onset. These mechanisms explain why bulk GaAs exhibits poor thermoelectric performance ($ZT < 0.1$) while nanoribbons achieve $ZT > 0.8$; the nanoscale geometry decouples typically competing transport parameters.[73]

For device applications, the predictions suggest distinct optimization strategies: Peltier cooling operates optimally at 100–200 K with heavy doping ($\mu \approx -1.0$ eV) to maximize the Seebeck coefficient; power generation achieves maximum efficiency at 400–550 K with moderate doping ($\mu \approx -1.5$ eV); and waste heat recovery benefits from broad temperature operation (300–500 K) with adaptive doping profiles. The model indicates that GaAs nanoribbons could achieve thermoelectric conversion efficiencies exceeding 8% at 500 K with $\Delta T = 200$ K, comparable to those of commercial Bi_2Te_3-based devices[73,74] with the advantage of higher temperature operation and III–V semiconductor compatibility.

While the ML predictions provide valuable insights, several limitations warrant consideration: (1) the model extrapolates from single-temperature (300 K) NEGF + DFTB data, requiring validation at multiple temperatures; (2) the $\kappa_{ph} \sim T^{-08}$ scaling approximates complex phonon scattering mechanisms; (3) bipolar conduction at very high temperatures (>600 K) could further degrade performance, which is neglected in the current model. Future work should incorporate temperature-dependent band structure calculations and experimental validation across the temperature range. Nevertheless, the combined NEGF + DFTB and ML approach successfully identifies optimal operating conditions and provides a framework for accelerated thermoelectric material optimization.[75]

IV. Conclusion

In summary, our comprehensive theoretical analysis establishes GaAs nanoribbons as exceptional candidates for thermoelectric energy conversion through an integrated approach combining first-principles NEGF + DFTB calculations with physics-informed machine learning predictions. The 300 K computational results reveal that quantum confinement-induced electronic resonances and phonon band gap-reduced thermal conductivity synergistically produce a remarkable figure of merit ($ZT > 0.6$).

Crucially, our machine learning model extends these findings beyond single-temperature calculations, predicting that thermoelectric performance exhibits a pronounced optimum at 450 K with ZT reaching 0.85—a 37% enhancement over room temperature. This ML-driven analysis identifies three distinct operational regimes governed by different physical mechanisms: quantum confinement preservation at cryogenic temperatures (<200 K) for an enhanced Seebeck coefficient, thermal activation at intermediate temperatures (200–400 K), and phonon engineering advantages at elevated temperatures (>400 K) that enable ZT enhancement despite the onset of bipolar conduction. The ML predictions further reveal temperature-dependent optimization strategies: cryogenic applications (100–200 K) benefit from heavy doping ($\mu \approx -1.0$ eV), while power generation (400–550 K) is optimized with moderate doping ($\mu \approx -1.5$ eV).

The integration of machine learning with first-principles calculations represents a significant methodological advancement, enabling efficient exploration of temperature-dependent phenomena that would be computationally prohibitive with NEGF + DFTB alone. This combined approach not only validates the theoretical potential of GaAs nanoribbons but also establishes a predictive framework that can accelerate the development of high-performance thermoelectric materials. Our findings provide concrete guidelines for experimental realization and device optimization, highlighting the transformative potential of III–V semiconductor nanostructures for next-generation thermoelectric applications.

Conflicts of interest

The authors declare that they have no known competing financial interests or personal relationships that could have appeared to influence the work reported in this paper.

Data availability

The original contributions presented in this study are included in the article. Further inquiries can be directed to the corresponding author.

Acknowledgements

S. Goumri-Said thanks the office of research at Alfaisal University in Saudi Arabia for funding this research work through internal project number 24407. M. B. Kanoun would like to thank Prince Sultan University for their support.

References

1 K. S. Novoselov, A. K. Geim, S. V. Morozov, *et al.*, Electric field effect in atomically thin carbon films, *Science*, 2004, **306**, 666–669, DOI: 10.1126/science.1102896.
2 Y. B. Zhang, Y. W. Tan, H. L. Stormer and P. Kim, Experimental observation of the quantum Hall effect and Berry's phase in graphene, *Nature*, 2005, **438**, 201–204, DOI: 10.1038/nature04235.
3 X. Li, X. Wang, L. Zhang, S. Lee and H. Dai, Chemically derived, ultrasmooth graphene nanoribbon semiconductors, *Science*, 2008, **319**, 1229–1232, DOI: 10.1126/science.1150878.
4 Y. M. Zuev, W. Chang and P. Kim, Thermoelectric and magnetothermoelectric transport measurements of graphene, *Phys. Rev. Lett.*, 2009, **102**, 096807, DOI: 10.1103/PhysRevLett.102.096807.
5 T. Löfwander and M. Fogelström, Impurity scattering and Mott's formula in graphene, *Phys. Rev. B:Condens. Matter Mater. Phys.*, 2007, **76**, 193401, DOI: 10.1103/PhysRevB.76.193401.
6 E. H. Hwang, E. Rossi and S. Das Sarma, Theory of thermopower in two-dimensional graphene, *Phys. Rev. B:Condens. Matter Mater. Phys.*, 2009, **80**, 235415, DOI: 10.1103/PhysRevB.80.235415.
7 A. I. Hochbaum, R. Chen, R. D. Delgado, W. Liang, E. C. Garnett, M. Najarian, A. Majumdar and P. Yang, Enhanced thermoelectric performance of rough silicon nanowires, *Nature*, 2008, **451**, 163–167, DOI: 10.1038/nature06381.
8 A. I. Boukai, Y. Bunimovich, J. Tahir-Kheli, J.-K. Yu, W. A. Goddard and J. R. Heath, Silicon nanowires as efficient thermoelectric materials, *Nature*, 2008, **451**, 168–171, DOI: 10.1038/nature06458.
9 T. Markussen, A. P. Jauho and M. Brandbyge, Electron and phonon transport in silicon nanowires: atomistic approach to thermoelectric properties, *Phys. Rev. B:Condens. Matter Mater. Phys.*, 2009, **79**, 035415, DOI: 10.1103/PhysRevB.79.035415.
10 S. Datta, *Quantum Transport: Atom to Transistor*, Cambridge University Press, Cambridge, 2005, DOI: 10.1017/CBO9781139164313.
11 Y. Sun, V. Kumar, I. Adesida and J. Rogers, Buckled and wavy ribbons of GaAs for high-performance electronics on elastomeric substrates, *Adv. Mater.*, 2006, **18**, 2857–2862, DOI: 10.1002/adma.200600646.
12 Y. Wang, Y. Chen, H. Li, *et al.*, Buckling-based method for measuring the strain–photonic coupling effect of GaAs nanoribbons, *ACS Nano*, 2016, **10**, 8199–8206, DOI: 10.1021/acsnano.6b03434.
13 Y. Hu, P. Xie, M. De Corato, *et al.*, Bandgap engineering of graphene nanoribbons by control over structural distortion, *J. Am. Chem. Soc.*, 2018, **140**, 7803–7809, DOI: 10.1021/jacs.8b02209.
14 C. Liu, B. Yao, T. Dong, *et al.*, Highly stretchable graphene nanoribbon springs by programmable nanowire lithography, *npj 2D Mater. Appl.*, 2019, **3**, 23, DOI: 10.1038/s41699-019-0105-7.
15 P. Moles, H. Santos, F. Domínguez-Adame and L. Chico, Tuning magnetism in graphene nanoribbons via strain and adatoms, *Phys. Rev. Res.*, 2025, **7**, 033255, DOI: 10.1103/6tny-vt8q.
16 Y. Ouyang and J. Guo, A theoretical study on thermoelectric properties of graphene nanoribbons, *Appl. Phys. Lett.*, 2009, **94**, 263107, DOI: 10.1063/1.3171933.
17 T. Yamamoto and K. Watanabe, Nonequilibrium Green's function approach to phonon transport in defective carbon nanotubes, *Phys. Rev. Lett.*, 2006, **96**, 255503, DOI: 10.1103/PhysRevLett.96.255503.
18 T. Markussen, A. P. Jauho and M. Brandbyge, Heat conductance is strongly anisotropic for pristine silicon nanowires, *Nano Lett.*, 2008, **8**, 3771–3775, DOI: 10.1021/nl8020889.
19 R. Saito, G. Dresselhaus and M. S. Dresselhaus, *Physical Properties of Carbon Nanotubes*, Imperial College Press, London, 2004, DOI: 10.1142/p080.
20 U. Sivan and Y. Imry, Multichannel Landauer formula for thermoelectric transport with application to thermopower near the mobility edge, *Phys. Rev. B:Condens. Matter Mater. Phys.*, 1986, **33**, 551–558, DOI: 10.1103/PhysRevB.33.551.
21 D. Gunlycke, H. M. Lawler and C. T. White, Room-temperature ballistic transport in narrow graphene strips, *Phys. Rev. B:Condens. Matter Mater. Phys.*, 2007, **75**, 085418, DOI: 10.1103/PhysRevB.75.085418.
22 D. K. Ferry, S. M. Goodnick and J. P. Bird, *Transport in Nanostructures*, Cambridge University Press, Cambridge, 2nd edn, 2012.
23 A. Arab, A. Davydov, D. Papaconstantopoulos and Q. Li, Monolayer MoS_2 nanoribbons as a promising material for both n-type and p-type legs in thermoelectric generators, *J. Electron. Mater.*, 2016, **45**, 5253–5263, DOI: 10.1007/s11664-016-4725-9.
24 Y. N. Peng, J. M. Liu, W. Y. Zhang, D. Wu, P.-Z. Jia, W.-X. Zhou and K.-Q. Chen, An efficient mechanism for

enhancing the thermoelectricity of twin graphene nanoribbons by introducing defects, *Phys. E*, 2020, **122**, 114160, DOI: 10.1016/j.physe.2020.114160.

25 B. Zhang, X. Zhang, S. Zhang, Y.-P. Wang, J. Dong, Y. Sun, F. Ouyang and M. Long, Modulation of thermoelectric performance of Cn-BTBT molecular junctions by engineering contact geometry, *Results Phys.*, 2021, **26**, 104318, DOI: 10.1016/j.rinp.2021.104318.

26 M. Brandbyge, J. L. Mozos, P. Ordejón, J. Taylor and K. Stokbro, Density-functional method for nonequilibrium electron transport, *Phys. Rev. B:Condens. Matter Mater. Phys.*, 2002, **65**, 165401, DOI: 10.1103/PhysRevB.65.165401.

27 B. K. Nikolić, K. K. Saha, T. Markussen and K. S. Thygesen, First-principles quantum transport modeling of thermoelectricity in nanoscale junctions, *J. Comput. Electron.*, 2012, **11**, 78–92, DOI: 10.1007/s10825-012-0386-y.

28 M. Luisier and G. Klimeck, Atomistic full-band simulations of silicon nanowire transistors: effects of electron-phonon scattering, *Phys. Rev. B:Condens. Matter Mater. Phys.*, 2009, **80**, 155430, DOI: 10.1103/PhysRevB.80.155430.

29 S. Smidstrup, K. Stokbro, A. Blom, *et al.*, QuantumATK: an integrated platform of electronic and atomic-scale modelling tools, *J. Phys.:Condens. Matter*, 2020, **32**, 015901, DOI: 10.1088/1361-648X/ab4007.

30 J. P. Perdew, K. Burke and M. Ernzerhof, Generalized gradient approximation made simple, *Phys. Rev. Lett.*, 1996, **77**, 3865–3868, DOI: 10.1103/PhysRevLett.77.3865.

31 S. Baroni, S. de Gironcoli, A. Dal Corso and P. Giannozzi, Phonons and related crystal properties from density-functional perturbation theory, *Rev. Mod. Phys.*, 2001, **73**, 515–562, DOI: 10.1103/RevModPhys.73.515.

32 S. S. Chauhan, P. Srivastava and A. K. Shrivastava, Band gap engineering in doped graphene nanoribbons: an ab initio approach, *Solid State Commun.*, 2013, **154**, 69–71, DOI: 10.1016/j.ssc.2012.10.030.

33 S. Yamacli and M. Avci, Simple and accurate model for voltage-dependent resistance of metallic carbon nanotube interconnects: an ab initio study, *Phys. Lett. A*, 2009, **374**, 297–304, DOI: 10.1016/j.physleta.2009.10.043.

34 M. A. S. Sakr, M. A. Saad, H. Abdelsalam, N. H. Teleb and Q. Zhang, Electronic and optical properties of chemically modified 2D GaAs nanoribbons, *Sci. Rep.*, 2023, **13**, 15535, DOI: 10.1038/s41598-023-42855-y.

35 X. Xu, J. Wang, Z. Wang, F. Liu, Y. Ye, Y. Zhang, P. Wang, P. Gao, B. Shen and X. Wang, Phonon dispersion of buckled two-dimensional GaN, *Nat. Commun.*, 2024, **15**, 10436, DOI: 10.1038/s41467-024-54921-8.

36 B. Song, S. Huang, J. Zhou, M. Li, Y. Dong, H. Zhou, J. Garlow, L. Wu, B. J. Kirby, A. J. Grutter, A. A. Puretzky, Y. Zhu, M. S. Dresselhaus, A. Gossard and G. Chen, Phonon localization in heat conduction, *Sci. Adv.*, 2018, **4**, eaat9460, DOI: 10.1126/sciadv.aat9460.

37 T. H. Wang and H. T. Horng, Topological thermal transport properties of graphene nanoribbons, *Int. J. Heat Mass Tran.*, 2019, **138**, 718–725, DOI: 10.1016/j.ijheatmasstransfer.2019.04.092.

38 B. Bhakti, S. Datta, A. Ghosh and M. Ghosh, Subtle modulation of the nonlinear optical properties of GaAs quantum dot by the interplay between noise and impurity extension, *Eur. Phys. J. B*, 2025, **98**, 25, DOI: 10.1140/epjb/s10051-025-00880-y.

39 Y. Chen, T. Jayasekera, A. Calzolari, K. W. Kim and M. Buongiorno Nardelli, Thermoelectric properties of graphene nanoribbons junctions, *J. Phys.:Condens. Matter*, 2010, **22**, 372202, DOI: 10.1088/0953-8984/22/37/372202.

40 M. El-Saba, Carrier transport in low-dimensional semiconductors (LDSs), in *Transport of Information-Carriers in Semiconductors and Nanodevices*, IGI Global, 2017, p. 274–333, DOI: 10.4018/978-1-5225-2312-3.ch005.

41 S. Fust, A. Faustmann, D. J. Carrad, J. Bissinger, B. Loitsch, M. Döblinger, J. Becker, G. Abstreiter, J. J. Finley and G. Koblmüller, Quantum-confinement-enhanced thermoelectric properties in modulation-doped GaAs–AlGaAs core–shell nanowires, *Adv. Mater.*, 2020, **32**, 1905458, DOI: 10.1002/adma.201905458.

42 L. Chen, Z. Ma, J. C. Cao, T. Y. Zhang and C. Zhang, Phonon-limited mobility in two-dimensional semiconductors with spin-orbit coupling, *Appl. Phys. Lett.*, 2007, **91**, 102115, DOI: 10.1063/1.2783203.

43 W. Zhou, K. Yamamoto, A. Miura, R. Iguchi, Y. Miura, K.-i Uchida and Y. Sakuraba, Seebeck-driven transverse thermoelectric generation, *Nat. Mater.*, 2021, **20**, 463–467, DOI: 10.1038/s41563-020-00884-2.

44 X. Jiang, Q. Xiong, S. Nam, *et al.*, InAs nanowire field-effect transistors with multiple independent wrap-gate segments, *Nano Lett.*, 2007, **7**, 3214–3218, DOI: 10.1021/nl072024a.

45 Y. C. Hua and B. Y. Cao, Study of phononic thermal transport across nanostructured interfaces using phonon Monte Carlo method, *Int. J. Heat Mass Tran.*, 2020, **154**, 119678, DOI: 10.1016/j.ijheatmasstransfer.2020.119762.

46 J. Zhang, Y. Hong and Y. Yue, Thermal transport across graphene and single layer hexagonal boron nitride, *J. Appl. Phys.*, 2015, **117**(13), 134307, DOI: 10.1063/1.4916985.

47 X. Lu, Q. Zhang, J. Liao, H. Chen, Y. Fan, J. Xing, S. Gu, J. Huang, J. Ma, J. Wang, L. Wang and W. Jiang, High-efficiency thermoelectric power generation enabled by homogeneous incorporation of MXene in $(Bi,Sb)_2Te_3$ matrix, *Adv. Energy Mater.*, 2020, **10**, 1902986, DOI: 10.1002/aenm.201902986.

48 W. Zuo, H. Chen, Z. Yu, *et al.*, Atomic-scale interface strengthening unlocks efficient and durable Mg-based thermoelectric devices, *Nat. Mater.*, 2025, **24**, 123–134, DOI: 10.1038/s41563-025-02167-0.

49 X. Cheng, Z. Ji, X. Yang, X. Wang, D. Han, M. Wang and W. Ding, Enhancement of thermoelectric performance in monolayer AlP_3 via Ga and In doping: a first-principles study, *Mater. Sci. Semicond. Process.*, 2024, **176**, 108332, DOI: 10.1016/j.mssp.2024.108332.

50 L. Xu, M. Yang, S. J. Wang and Y. P. Feng, Electronic and optical properties of the monolayer group-IV monochalcogenides MX (M = Ge, Sn; X = S, Se, Te), *Phys. Rev. B*, 2017, **95**, 235434, DOI: 10.1103/PhysRevB.95.235434.

51 A. Giri, S. G. Walton, J. Tomko, N. Bhatt, M. J. Johnson, D. R. Boris, G. Lu, J. D. Caldwell, O. V. Prezhdo and P. E. Hopkins, Ultrafast and nanoscale energy transduction mechanisms and coupled thermal transport across interfaces, *ACS Nano*, 2023, **17**, 14253–14282, DOI: 10.1021/acsnano.3c02417.

52 A. Li, Y. Wang, Y. Li, X. Yang, P. Nan, K. Liu, B. Ge, G. Fu and T. Zhu, High performance magnesium-based plastic semiconductors for flexible thermoelectrics, *Nat. Commun.*, 2024, **15**, 5108, DOI: 10.1038/s41467-024-49440-5.

53 P. Avouris, Graphene: electronic and photonic properties and devices, *Nano Lett.*, 2010, **10**, 4285–4294, DOI: 10.1021/nl102824h.

54 E. R. Mucciolo, A. H. Castro Neto and C. H. Lewenkopf, Conductance quantization and transport gaps in disordered graphene nanoribbons, *Phys. Rev. B:Condens. Matter Mater. Phys.*, 2009, **79**, 075407, DOI: 10.1103/PhysRevB.79.075407.

55 M. Yagmurcukardes, F. M. Peeters, R. T. Senger and H. Sahin, Nanoribbons: from fundamentals to state-of-the-art applications, *Appl. Phys. Rev.*, 2016, **3**, 041302, DOI: 10.1063/1.4966963.

56 Y. H. Xu, Z. Q. Fan, Z. H. Zhang and T. Zhao, Electronic and transport properties of GaAs/InSe van der Waals heterostructure, *Appl. Surf. Sci.*, 2021, **547**, 149174, DOI: 10.1016/j.apsusc.2021.149174.

57 M. Q. Zhu and X. F. Wang, Edge-modified zigzag GeS nanoribbon devices with tunable electronic properties and significant negative differential resistance effect: a first-principle study, *Surf. Interfaces*, 2024, **46**, 104201, DOI: 10.1016/j.surfin.2024.104201.

58 H. Wang, H. S. Wang, C. Ma, *et al.*, Graphene nanoribbons for quantum electronics, *Nat. Rev. Phys.*, 2021, **3**, 791–802, DOI: 10.1038/s42254-021-00370-x.

59 J. Schmidt, M. R. G. Marques, S. Botti and M. A. L. Marques, Recent advances and applications of machine learning in solid-state materials science, *npj Comput. Mater.*, 2019, **5**, 83, DOI: 10.1038/s41524-019-0221-0.

60 K. T. Butler, D. W. Davies, H. Cartwright, O. Isayev and A. Walsh, Machine learning for molecular and materials science, *Nature*, 2018, **559**(7715), 547–555, DOI: 10.1038/s41586-018-0337-2.

61 G. Pilania, C. Wang, X. Jiang, S. Rajasekaran and R. Ramprasad, Accelerating materials property predictions using machine learning, *Sci. Rep.*, 2013, **3**, 2810, DOI: 10.1038/srep02810.

62 L. D. Hicks and M. S. Dresselhaus, Effect of quantum-well structures on the thermoelectric figure of merit, *Phys. Rev. B:Condens. Matter Mater. Phys.*, 1993, **47**(19), 12727–12731, DOI: 10.1103/PhysRevB.47.12727.

63 A. I. Hochbaum, R. Chen, R. D. Delgado, *et al.*, Enhanced thermoelectric performance of rough silicon nanowires, *Nature*, 2008, **451**(7175), 163–167, DOI: 10.1038/nature06381.

64 G. D. Mahan, Good thermoelectrics, *Solid State Phys.*, 1998, **51**, 81–157.

65 M. S. Dresselhaus, G. Chen, M. Y. Tang, *et al.*, New directions for low-dimensional thermoelectric materials, *Adv. Mater.*, 2007, **19**(8), 1043–1053, DOI: 10.1002/adma.200600527.

66 Y. Pei, X. Shi, A. LaLonde, H. Wang, L. Chen and G. J. Snyder, Convergence of electronic bands for high performance bulk thermoelectrics, *Nature*, 2011, **473**(7345), 66–69, DOI: 10.1038/nature09996.

67 G. J. Snyder and E. S. Toberer, Complex thermoelectric materials, *Nat. Mater.*, 2008, **7**(2), 105–114, DOI: 10.1038/nmat2090.

68 T. C. Harman, P. J. Taylor, M. P. Walsh and B. E. LaForge, Quantum dot superlattice thermoelectric materials and devices, *Science*, 2002, **297**(5590), 2229–2232, DOI: 10.1126/science.1072886.

69 J. P. Heremans, V. Jovovic, E. S. Toberer, *et al.*, Enhancement of thermoelectric efficiency in PbTe by distortion of the electronic density of states, *Science*, 2008, **321**(5888), 554–557, DOI: 10.1126/science.1159725.

70 A. J. Minnich, M. S. Dresselhaus, Z. F. Ren and G. Chen, Bulk nanostructured thermoelectric materials: current research and future prospects, *Energy Environ. Sci.*, 2009, **2**(5), 466–479, DOI: 10.1039/b822664b.

71 J. Ma, O. Delaire, A. F. May, *et al.*, Glass-like phonon scattering from a spontaneous nanostructure in $AgSbTe_2$, *Nat. Nanotechnol.*, 2013, **8**(6), 445–451, DOI: 10.1038/nnano.2013.95.

72 M. Zebarjadi, K. Esfarjani, M. S. Dresselhaus, Z. F. Ren and G. Chen, Perspectives on thermoelectrics: from fundamentals to device applications, *Energy Environ. Sci.*, 2012, **5**(1), 5147–5162, DOI: 10.1039/C1EE02497C.

73 B. Poudel, Q. Hao, Y. Ma, *et al.*, High-thermoelectric performance of nanostructured bismuth antimony telluride bulk alloys, *Science*, 2008, **320**(5876), 634–638, DOI: 10.1126/science.1156446.

74 K. F. Hsu, S. Loo, F. Guo, *et al.*, Cubic $AgPb_mSbTe_{2+m}$: bulk thermoelectric materials with high figure of merit, *Science*, 2004, **303**(5659), 818–821, DOI: 10.1126/science.1092963.

75 L. E. Bell, Cooling, heating, generating power, and recovering waste heat with thermoelectric systems, *Science*, 2008, **321**(5895), 1457–1461, DOI: 10.1126/science.1158899.